Journal of Nuclear Materials 378 (2008) 45–54

Contents lists available at ScienceDirect

Journal of Nuclear Materials

journal homepage: www.elsevier.com/locate/jnucmat

Kinetic parameters of the oxidation of zirconium alloys in simulated WWER water – Effect of KOH content

Martin Bojinov [a,*], Wei Cai [b], Petri Kinnunen [b], Timo Saario [b]

[a] Department of Physical Chemistry, University of Chemical Technology and Metallurgy, Kl. Ohridski Blvd. 8, 1756 Sofia, Bulgaria
[b] VTT Materials and Building, VTT Technical Research Centre of Finland, P.O. Box 1000, Kemistintie 3, FIN-02044 VTT, Espoo, Finland

ARTICLE INFO

Article history:
Received 10 January 2008
Accepted 24 April 2008

ABSTRACT

The pre-transition oxides formed on two different types of zirconium alloys (Zircaloy 4 and E110) have been characterised in situ using electrochemical impedance spectroscopy (EIS) in high-temperature electrolyte simulating WWER conditions at 310 °C. To obtain a correlation between the oxide film thickness, the oxide growth rate and the impedance parameters, the EIS data have been fitted to a transfer function derived from the mixed-conduction model for oxide films, allowing for the contribution of both an inner, barrier type of oxide and a more defective outer layer. The values of the total oxide film thickness based on the model calculations have proved to be in a good agreement with the values measured from the cross-section micrographs of the specimens using scanning electron microscopy. The main kinetic and transport parameters characterising the oxidation process have been estimated and discussed with regard to the effect of KOH content and alloy type on the mechanism of conduction through the formed oxide.

1. Introduction

There is considerable interest towards the mechanism of oxide film growth and corrosion of zirconium alloys used as fuel cladding materials in nuclear reactors. The tendency towards more severe operating conditions induced by the need for longer service times and higher fuel burnups has called for a more thorough characterisation of the relationship between the composition and microstructure of the Zr alloys, their oxide growth kinetics and susceptibility to localised corrosion modes [1–4]. The elevated lithium concentration is necessary in pressurised water reactors (PWRs) with high burnup and longer than 12-month fuel cycles in order to keep the pH of the primary coolant within the optimal range. Elevated lithium concentration combined with local subcooled nucleate boiling accentuated by high burnup may result in formation of crud onto fuel cladding surfaces and further in the phenomenon called crud induced power shift (CIPS, previously called axial offset anomaly, AOA) or localised clad corrosion. The exact mechanism of CIPS is not known and numerous studies of this phenomenon have been and are being carried out (e.g. in the IAEA's *Optimisation of Water Chemistry to ensure Reliable Water Reactor Fuel Performance at High Burnup and in Aging Plant (FUWAC) 2006–2010* – programme) to clarify the relationship between fuel cladding materials, water chemistries and the occurrence of CIPS. However, several studies have proposed that there may be a connection between the alkali and boron concentrations, the composition of the fuel cladding materials and the occurrence of CIPS.

Despite of the fact that there is a general agreement on the oxidation process of zirconium alloys in high-temperature water, the exact mechanism of conduction through the oxide has remained unidentified. It is usually believed that the growth of the oxide proceeds according to the coupled-currents mechanism [2], in which the transport of oxygen vacancies along the grain boundaries of the zirconium oxide is the rate-limiting step of the overall reaction. Reduction of water at the oxide/electrolyte interface is assumed to consume electrons supplied by the oxidation of zirconium. It has been proposed that the electronic conduction through the oxide proceeds via easy paths associated with second phase particles embedded in the oxide matrix [1,3] or is due to the semiconductor properties of the formed oxide [5]. The extent of coupling between the electronic and ionic fluxes has remained largely unquantified.

In recent years, electrochemical impedance spectroscopy (EIS) has been extensively used to characterise the oxide films on zirconium alloys [6–23]. However, mainly ex situ measurements in aqueous electrolytes at room temperature, or experiments in a gaseous atmosphere following oxidation in high-temperature water have been reported. Only few measurements to follow the oxide growth in situ in pressurised water reactor (PWR) coolant conditions have been carried out. The most comprehensive of these studies has been focused on the impedance behaviour of Zircaloy 4 after long-term exposure to high-temperature lithiated water [17]. However, the interpretational part of that study has been focused on the high-frequency part of the impedance spectra in

* Corresponding author.
E-mail address: mbojinov@yahoo.com (M. Bojinov).

0022-3115/$ - see front matter © 2008 Elsevier B.V. All rights reserved.
doi:10.1016/j.jnucmat.2008.04.014

order to be able to follow the evolution of the thickness of the inner and outer layers of the formed oxide with time of exposure. The limited number of studies of zirconium alloys in water cooled water moderated energy reactor (WWER) coolants has effectively suffered by similar interpretational limitations [15,16,19]. Summarising, interpretations of the impedance spectra have usually focused on the dielectric or semiconductor properties of the oxide film, using mostly the equivalent circuit analysis approach. Only a few very recent investigations try to make a distinction between these characteristics and the transport processes due to the mixed conduction in the oxide. It is probable that no attempt has yet been made to correlate the impedance response to the oxide growth rate, which is believed to be proportional to the flux of oxygen vacancies in the already formed zirconium oxide.

Very recently, a kinetic approach to the anodic behaviour of pure Zr in both deaerated and hydrogenated boric acid–lithium hydroxide solutions has been proposed on the basis of the point defect model (PDM) and validated against EIS data obtained at 250 °C [22,23]. On the other hand, some of us have adapted the mixed-conduction model (MCM) for oxide films [24,25] to quantitatively describe the in situ impedance data for several Zircaloy 2-type alloys in simulated boiling water reactor (BWR) coolant at 300 °C [20]. As a consequence, several important kinetic and transport parameters of the growing oxide have been estimated. The values obtained for the oxide film thickness on the basis of model calculations were in a good agreement with the experimental values estimated from scanning electron microscopy (SEM) micrographs, and the ratio of the calculated oxide formation rates for the respective alloys corresponded well to the ratio of their in-reactor corrosion behaviour. A possible correlation between the inverse of the corrosion rate and the number of small second phase particles (SPP) found in the alloy matrix has been also proposed.

In the present work EIS measurements on two zirconium alloys typically used in WWER plants (Zircaloy 4 and E110) are used to check whether different water chemistry conditions (in the specific case, KOH concentration) will have an effect on the oxidation processes. The other goal in the studies carried out with different fuel cladding materials is to check whether differences in oxidation behaviour between different alloys can be distinguished already during pre-transition oxidation. If the comparison of corrosion behaviour on these materials could be performed reliably already during the pre-transition oxidation, the number of long-lasting and expensive post-transition oxidation tests could be decreased. The EIS results obtained during a 5-day exposure of the alloys to WWER water with different KOH content at 310 °C are interpreted using a modified version of the MCM and the main kinetic and transport parameters are estimated by fitting the spectra to the model equations. The obtained parameter values are discussed in terms of the effect of KOH concentration and alloy type on the kinetics of oxidation and the conduction mechanism of the formed oxide.

2. Experimental

The materials used in this study were Zircaloy 4 (Westinghouse, USA, nominal alloy composition, wt%: Sn 1.50, Fe 0.20, Cr 0.10, Ni < 0.007, balance Zr), and E110 (Zr–1%Nb, Chapetsky Mechanical Plant, Russia, nominal alloy composition, wt%: Nb 1.00, Sn < 0.01, Fe 0.014, Cr < 0.003, Ni < 0.004, C < 40–70 wppm, Si 46–90 wppm, N < 30–40 wppm, Hf 300–400 wppm, balance Zr). The disc-shaped specimens were cut from as-fabricated tubes by a diamond saw. The edges of the discs (Ø5.5 mm) were rounded with a side cutter. To prepare the working electrodes for the electrochemical measurements, a zirconium wire was spot-welded to the backside of the specimens and mechanically connected to a silver-plated copper wire. All the electrical connections were insulated using multilayer PTFE tape. The area of the samples exposed to the WWER coolant was estimated to be 0.5 cm^2. The samples were exposed to simulated WWER water prepared from H_3BO_3 (1200 ppm B), and KOH (11, 28 and 56 ppm K), 40 cm^3/kg H_2 (STP). All experiments were performed at 310 °C in an autoclave connected to a high-temperature water re-circulation loop. All the measurements were at least triplicated in order to ensure the reproducibility of the obtained results.

Electrochemical impedance spectra were measured by a Solartron 1287/1260 system controlled by ZPlot/ZView software (Scribner Associates) in a semicontinuous fashion during the 1–5 days of exposure to the simulated WWER water. Ir was used as both counter and pseudo-reference electrode in analogy to previous measurements [20]. The contribution of the Ir electrode to the impedance has been found to be less than 3% over the whole frequency range as estimated by measuring the impedance of an Ir–Ir couple in similar conditions. The frequency range in the measurements was from 80 kHz to 0.001 Hz and the amplitude of the a.c. perturbation was 50 mV (rms). The difference in the d.c. potential between the working and the counter electrode was ca. 20–30 mV. The validity of the impedance spectra was ensured by checking the linearity condition, i.e. measuring spectra at signal amplitudes between 5 and 50 mV (rms), and by checking the causality using a Kramers–Kronig compatibility (KK) test included in the ZView software. The reproducibility of the impedance spectra was ±2% by magnitude and ±3° by phase angle. After the impedance measurements the specimens were removed from the autoclave to estimate the total thickness of the oxides by SEM. For the simulation and fitting of impedance spectra to the transfer function derived from the kinetic model, Microcal Origin-based software was employed.

3. Results

The electrochemical impedance spectra of E110 and Zircaloy 4 in simulated WWER water with different KOH contents (11, 28 and 56 ppm) at 310 °C as depending on the time of exposure are presented in Figs. 1–6, respectively. Following our previous work [20], Bode representations of the spectra were adopted in order to be able to discern clearly the impedance signatures at both high and low frequencies. Results of several repetitive runs are included in some of the figures to demonstrate the reproducibility of the obtained spectra.

The magnitude of the impedance at low frequencies (e.g. 0.001 Hz) $Z_{f\to 0}$ that can be interpreted as the inverse of the steady-state conductivity of the alloy/oxide/electrolyte system, in general increases with exposure time, indicating that oxide growth is taking place. The increase of $Z_{f\to 0}$ is not very pronounced, indicating that oxide growth is slow and the system can be regarded as being in a quasi-steady-state with respect to the measurement time of a single impedance spectrum. The fact that the time evolution of the system was negligible with respect to measurement time was corroborated by the fact that all the presented impedance spectra passed the Kramers-Kronig transform test. In general, $Z_{f\to 0}$ is larger for the films formed on E110 when compared to those on Zircaloy 4 for a constant exposure time, indicating that the rate of the limiting step of the oxidation process (most probably the dissolution of the already formed oxide) is smaller for the former alloy. On the other hand, $Z_{f\to 0}$ decreases with the increase in KOH content of the electrolyte, this decrease being more pronounced for the oxides formed on Zircaloy 4 when compared to those on E110. Thus increasing the KOH concentration in the electrolyte leads to an increase in the rate of the limiting step of oxidation,

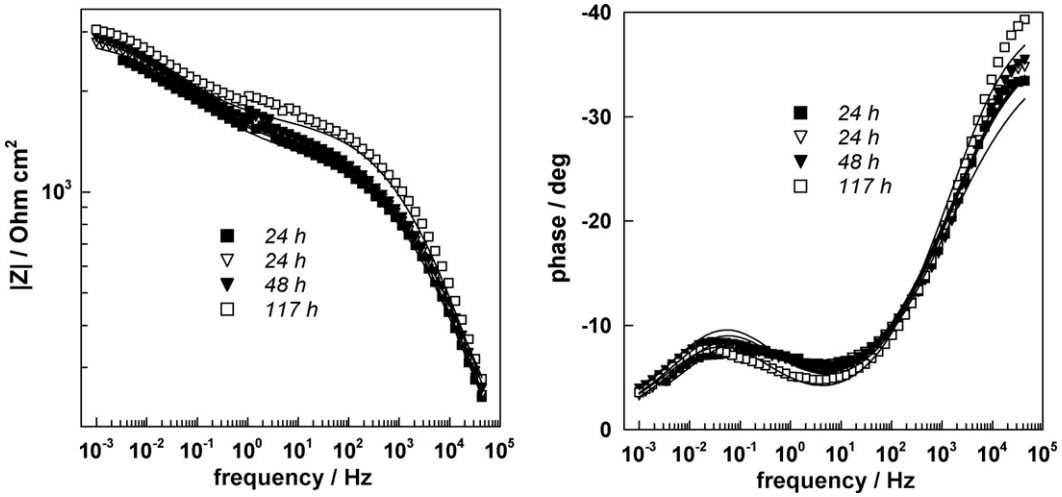

Fig. 1. Electrochemical impedance spectra of E110 in simulated WWER water (11 ppm KOH) at 310 °C as depending on the exposure time. Left – impedance magnitude vs. frequency, right – phase angle vs. frequency. Points – experimental values, solid lines – best-fit calculation according to the proposed model.

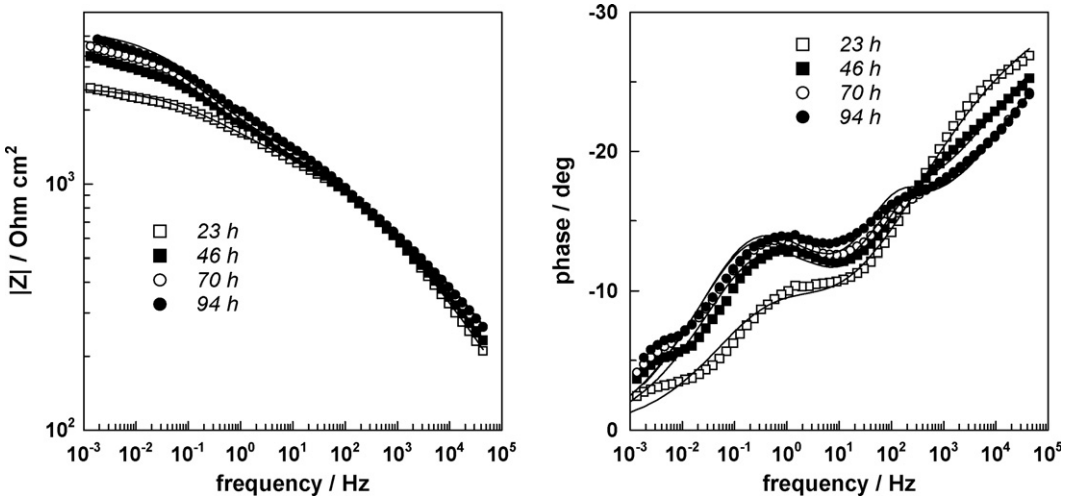

Fig. 2. Electrochemical impedance spectra of Zircaloy 4 in simulated WWER water (11 ppm KOH) at 310 °C as depending on the exposure time. Left – impedance magnitude vs. frequency, right – phase angle vs. frequency. Points – experimental values, solid lines – best-fit calculation according to the proposed model.

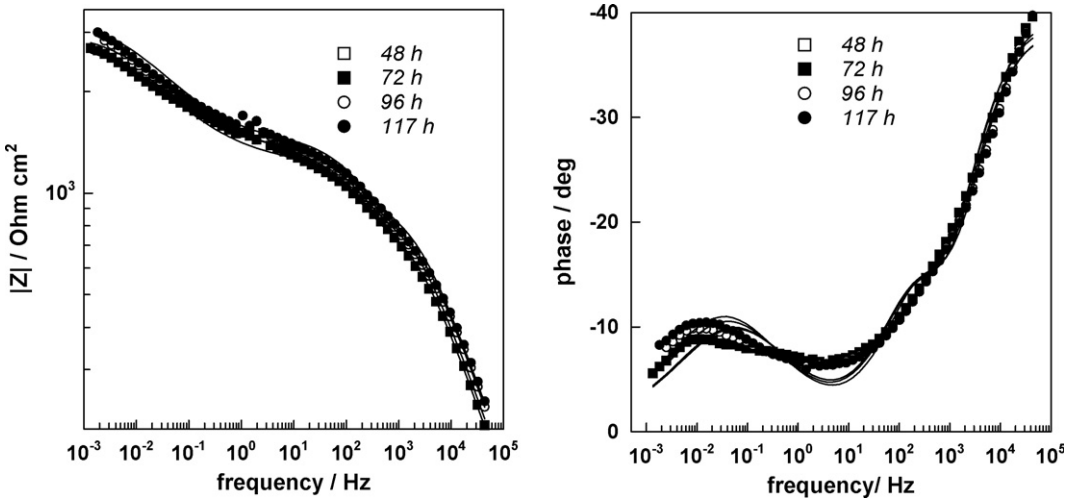

Fig. 3. Electrochemical impedance spectra of E110 in simulated WWER water (28 ppm KOH) at 310 °C as depending on the exposure time. Left – impedance magnitude vs. frequency, right – phase angle vs. frequency. Points – experimental values, solid lines – best-fit calculation according to the proposed model.

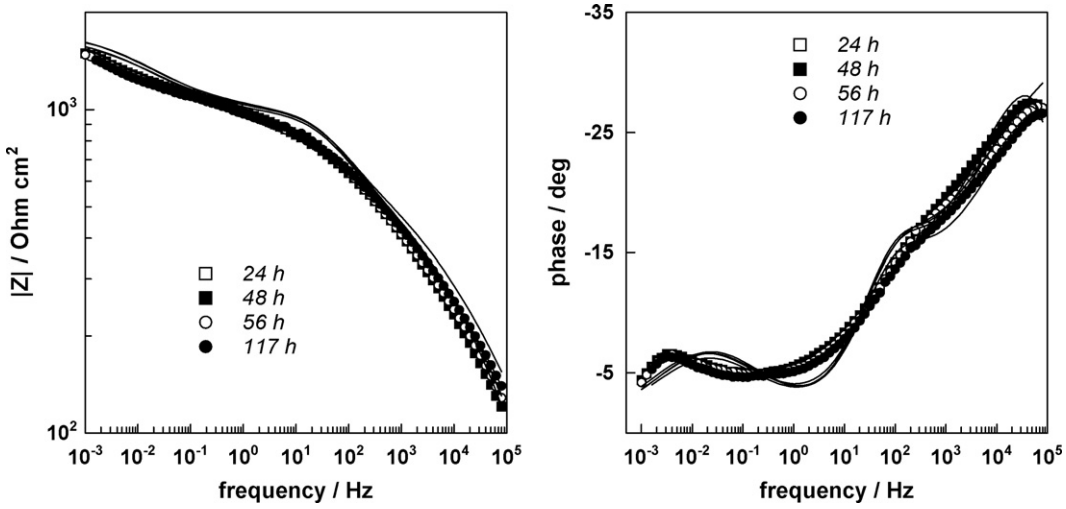

Fig. 4. Electrochemical impedance spectra of Zircaloy 4 in simulated WWER water (28 ppm KOH) at 310 °C as depending on the exposure time. Left – impedance magnitude vs. frequency, right – phase angle vs. frequency. Points – experimental values, solid lines – best-fit calculation according to the proposed model.

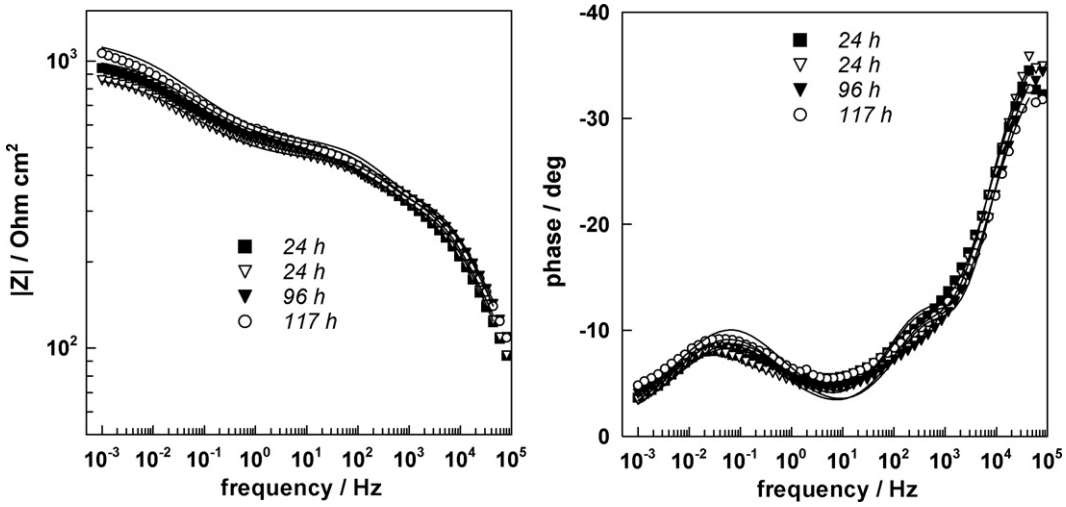

Fig. 5. Electrochemical impedance spectra of E110 in simulated WWER water (56 ppm KOH) at 310 °C as depending on the exposure time. Left – impedance magnitude vs. frequency, right – phase angle vs. frequency. Points – experimental values, solid lines – best-fit calculation according to the proposed model.

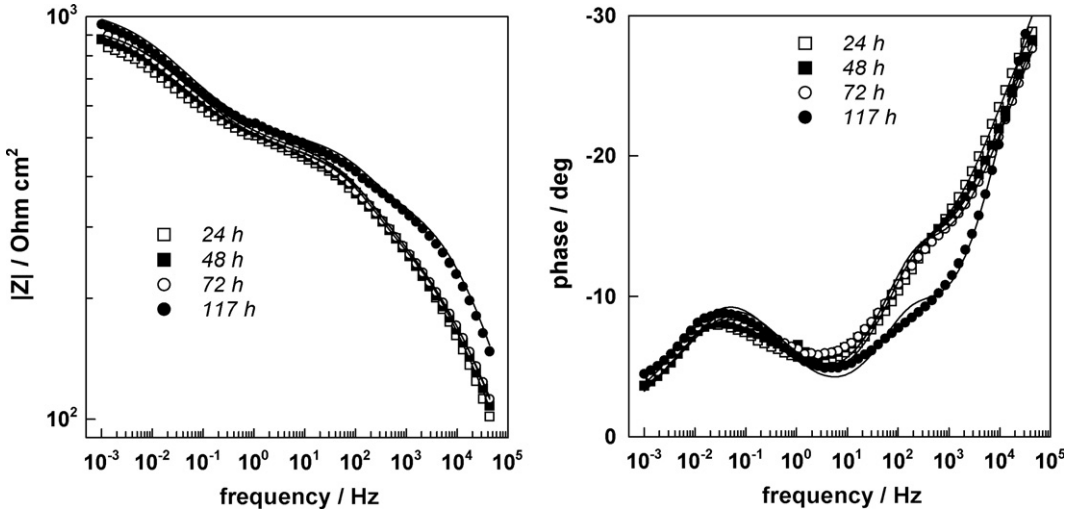

Fig. 6. Electrochemical impedance spectra of Zircaloy 4 in simulated WWER water (56 ppm KOH) at 310 °C as depending on the exposure time. Left – impedance magnitude vs. frequency, right – phase angle vs. frequency. Points – experimental values, solid lines – best-fit calculation according to the proposed model.

which has been found to be analogous to similar measurements performed by us in simulated PWR water with different LiOH content (unpublished). At this stage, it can be argued that the increase in KOH concentration is increasing the solubility of the zirconium oxide at its interface with the electrolyte, therefore the quasi-steady-state is reached at a larger respective rate of oxide growth to compensate for dissolution. This finding implies that either solubility or dissolution rate of the oxide appear to be corrosion rate limiting, as proposed by Markworth et al. [26] for the corrosion of Zr–2.5Nb alloy in Canadian Deuterium Uranium (CANDU) coolants. In the model devised by these authors, the zirconium oxide layer is treated as a bilayer with an inner protective barrier and an outer porous nonprotective layer. The transformation of the barrier layer into a nonprotective porous layer at the outer side of the barrier layer ultimately controls the reaction, because the thickness of the barrier layer is dependent on this transformation. Similar work has been reported by Macdonald and co-workers [22,23,27] on oxide films in which the steady-state growth and dissolution of the barrier layer was studied.

A total of three time constants is observed in the phase angle vs. frequency curves in a certain analogy to the results published by Schefold et al. in simulated PWR water at 360 °C [10]. The time constant situated at the highest frequencies (ca. 10–30 kHz) can be related to the electric properties of the outer layer of oxide, that observed at intermediate frequencies (100–500 Hz) to the electric properties of the inner, protective barrier layer, whereas the lowest frequency time constant situated below 0.1 Hz is most probably due to a solid state diffusion-migration process (transport of oxygen vacancies in the barrier layer) [20–23]. In general, the characteristic frequencies of the highest-frequency time constant increase with the time of exposure and also with KOH content in the electrolyte, indicating a larger thickness of the outer layer. In principle, the characteristic frequencies of the medium frequency time constant also increase with exposure time, but their evolution with KOH concentration is more difficult to discern because of the overlap of the time constants related to the properties of the two layers of oxide. On the other hand, no meaningful evolution of the characteristic frequency of the time constant associated with the transport process could be observed. This fact could be related to the fact that the transport properties of the barrier layer are not so significantly affected by either the exposure time or KOH concentration. However, a certain increase of this characteristic frequency could be observed for the oxides on both alloys when the KOH content is increased from 28 to 56 ppm, which could be related to an increase in the transport rate.

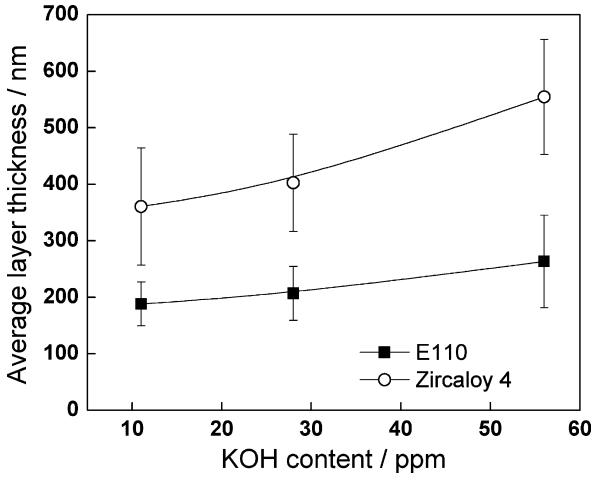

Fig. 7. Microscopic estimates of the oxide film thickness on E110 and Zircaloy 4 after 120 h of exposure to simulated WWER water as depending on the KOH content.

Fig. 7 presents the estimates of the film thickness on the studied samples of both alloys after 120 h exposure to the simulated WWER water at 310 °C obtained from microscopic examination of metallographic cross-sections. The thicknesses increase with KOH content, this increase being more pronounced when the concentration is changed from 28 to 56 ppm. Another important fact is that the thickness of the oxides on the Zircaloy 4 samples is significantly larger than that on E110 electrodes, the difference between the oxides on the two alloys becoming the larger, the higher the KOH content in the electrolyte. It is also worth noting that the variations in the oxide thickness increase with KOH content and are much more pronounced for the oxides Zircaloy 4.

Summarising, the in situ impedance measurements and the ex situ microscopic observations point to a significant effect of KOH concentration in the electrolyte on the kinetics of the oxidation process of zirconium alloys in simulated WWER water. The differences between the oxidation kinetics between the two alloys are also well discernible and are the more pronounced, the higher the KOH content in the solution. In order to be able to rationalise these facts in terms of the conduction mechanism of the alloy/oxide/water systems, a kinetic model of the oxidation process has to be developed and validated. An approach to such a model is described in the following section.

4. Discussion

4.1. Conceptual model

The qualitative picture of the zirconium alloy oxidation in high-temperature water suggests the following barrier layer growth reaction:

Alloy/barrier layer interface:

$$Zr_m \xrightarrow{k_1} Zr_{Zr} + 2V_O^{\cdot\cdot} + 4e' \quad \text{(zirconium oxidation)},$$

Barrier layer/water interface:

$$2V_O^{\cdot\cdot} + 2H_2O + 4e' \xrightarrow{k_2} 2O_O + 4H_{oxide}$$

(oxide formation and water reduction),

where Zr_m stands for a zirconium atom in the alloy, Zr_{Zr} and O_O are zirconium and oxygen ion positions in the ZrO_2 lattice, $V_O^{\cdot\cdot}$ is an oxygen vacancy in that lattice and k_1 and k_2 are the rate constants of the interfacial reactions. The above processes require the transport of oxygen vacancies and electrons through the oxide.

At the barrier layer/water interface, restructuring of that layer occurs and an outer layer is formed. This restructuring could proceed via dissolution, the rate of which is influenced by the concentration of KOH in analogy to what has been proposed by Markworth et al. [26] for the corrosion of Zr–2.5%Nb in high-temperature lithiated water

$$ZrO_2 + OH^- \xrightarrow{k_d} HZrO_3^-.$$

According to the PDM and the MCM the transport of oxygen vacancies in the oxide is governed by both diffusion and migration [22–25]:

$$J_O(x,t) = -D_O \frac{\partial c_O(x,t)}{\partial x} - 2KD_O c_O(x,t). \quad (1)$$

In this equation, $c_O(x,t)$ is the time and spatially dependent concentration of oxygen vacancies, $K = F\vec{E}/RT, \vec{E}$ is the electric field strength in the oxide and D_O is the diffusion coefficient of oxygen vacancies.

The steady-state solution of this equation with the boundary conditions $J_O(L) = k_1, J_O(0) = k_2 c_O(0)$ in a coordinate system in which $x = 0$ is at the barrier oxide/water interface at the bottom of the

pores of the outer layer and $x = L$ at the alloy/barrier layer interface, L being the barrier layer thickness, gives the concentration profile of oxygen vacancies in the barrier layer:

$$c_O(x) = 2k_1\left[\frac{e^{2Kx}}{k_2} + \frac{1}{2KD_O}\right]. \quad (2)$$

On the other hand, following other conceptual treatments of the oxide growth on zirconium alloys [1], the transport of matter and charge through the defective outer layer is assumed to take place by migration via short circuit paths like imperfections and cracks, or interconnected porosity. Thus no concentration gradient of oxygen vacancies is thought to be present in this layer and the transport mode through it is presumed to be pure ohmic migration.

4.2. Transfer function for the impedance response

The overall impedance of the alloy/barrier layer/outer layer/electrolyte system is written as

$$Z = R_{el} + Z_b + Z_{out}. \quad (3)$$

Several distributed impedance elements have been tried to simulate the impedance of the outer layer. The best results have been obtained with the so-called Havriliak–Negami response [28]

$$Z_{out} = \frac{R_{out}}{[1 + (j\omega R_{out}C_{out})^u]^n}, \quad (4)$$

where R_{out} and C_{out} are the apparent resistance and capacitance of the outer layer, and u and n are fractional exponents. The Havriliak–Negami response represents a generalisation of the constant phase element (CPE) to account for asymmetric capacitive loops. Mathematically, it also represents a good approximation to the Williams–Watts distribution [29]. This distribution has been found to agree rather well with the continuous random walk model of Scher and Lax for transport in disordered and composite media [16,19]. Interestingly, the Havriliak–Negami element has been proposed originally for polymer dispersions [28] and can be regarded according to the original authors as the impedance of a two phase mixture. This seems to represent a quite reasonable description for the ZrO_2 outer layer since it contains second phase particles in an otherwise homogeneous ZrO_2 matrix [1,3,4].

For the impedance of the barrier layer, the transfer function proposed earlier within the frames of the MCM [20] is employed

$$Z_b = (Z_e^{-1} + Z_{ion}^{-1})^{-1}, \quad (5)$$

where Z_e is the electronic contribution to the impedance of the inner barrier layer of oxide at the surface of the zirconium alloy. The electronic contribution to the impedance is related to the spatial variation of the steady-state concentration of oxygen vacancies in the oxide, which creates a positive ionic space charge that requires electronic compensation to achieve electroneutrality in the film. Thus, the electronic contribution to the impedance can be generally regarded as the non-ideal capacitance of a semiconductor layer with spatially and energetically variable defect density. An expression for Z_e has been derived using Eq. (2) as a starting point [20]:

$$Z_e = \frac{p}{j\omega C_b}\ln\left[\frac{1 + j\omega\rho_d\varepsilon\varepsilon_0 e^{1/p}}{1 + j\omega\rho_d\varepsilon\varepsilon_0}\right], \quad (6)$$

where $C_b = \frac{\varepsilon\varepsilon_0}{L_b}$, $\rho_d = \frac{RTk_1}{F^2D_ek_2}$, $p = \frac{1}{2KL_b}$, ε is the dielectric constant of zirconium oxide, assumed to be equal to 22 [1], ε_0 is the dielectric permittivity of free space, ω is the angular frequency and D_e is the diffusion coefficient of the electronic charge carriers.

On the other hand, the impedance due to the motion of ionic defects, Z_{ion}, can be obtained as the small amplitude ac solution of Eq. (1) in the form of a finite length Warburg impedance in series with a charge transfer resistance

$$Z_{ion} = R_t + \frac{RT}{4F^2KD_Oc_O(L)(1-\alpha)\left[1 + \sqrt{1 + \frac{j\omega}{K^2D_O}}\right]}, \quad (7)$$

where $c_O(L)$ is the concentration of oxygen vacancies at the alloy/barrier layer interface and α is the polarisability of the barrier layer/water interface [20,22,23]. This parameter characterises the part of the overall potential drop in the alloy/barrier layer/water system which is located at the barrier layer/water interface as opposed to film bulk. In the simplest case, it can be assumed that α 0, i.e. all the potential drop is located within the barrier layer of oxide. On the other hand, starting with Eq. (2), and assuming that $k_2e^{2KL} \gg 2KD_O$ [20], the concentration c_o (L) can be approximated as

$$c_O(L) = 2k_1\left[\frac{e^{-2KL}}{k_2} + \frac{1}{2KD_O}\right] \approx \frac{k_1}{KD_O}. \quad (8)$$

Finally, combining Eqs. (7) and (8), the equation for the impedance due to ionic transport becomes

$$Z_{ion} = R_t + \frac{RT}{4F^2k_1\left[1 + \sqrt{1 + \frac{j\omega}{K^2D_O}}\right]}. \quad (9)$$

The overall impedance is then calculated by taking into account Eqs. (3), (4), (6), (7) and (9).

4.3. Calculation procedure and parameter estimates

The spectra of both alloys in all the electrolyte combinations as depending on the time of exposure to simulated WWER water were quantitatively compared to the above transfer function using non-linear least square fitting. Statistical weighting was used for the experimental data set and the errors of parameter estimation were multiplied by the square root of the reduced chi-square value resulting from the fit. In spite of the relatively large number of parameters, this resulted in a sufficient number of degrees of freedom in the system in order to obtain statistically reliable values of the kinetic parameters. The calculated spectra are presented in Figs. 1–6 and demonstrate the ability of the proposed model to account for both the magnitude and the frequency distribution of the experimental impedances. The main discrepancies are observed in the lowest frequency region, in which the match between experiment and calculation is slightly worse. Bearing in mind the fact that we attempt to represent the transport in a disordered and heterogeneous medium using unidimensional linear diffusion-migration approach, at this stage the correspondence between model and experiments is considered satisfactory.

As a result of the fitting procedure, the parameters $R_{out}, C_{out}, C_b, \rho_d\varepsilon, k_1, D_O$, and $\vec{E}$ were estimated as depending on the alloy type, KOH content and exposure time. Due to the strong overlap of the time constants, the charge transfer resistance R_t could only be calculated with a relatively large error and is thus not commented further. Assuming a dielectric constant of 22, the thicknesses of the barrier and outer layers were computed from the respective capacitances. A collection of all the relevant parameters is presented in Fig. 8 (for the oxides formed on E110) and Fig. 9 (for the oxides formed on Zircaloy 4).

The following main conclusions can be drawn from the calculated parameter values:

- The estimates of the thickness of the whole oxide film from the capacitances of the inner and outer layers after 120 h of exposure agree very well with the estimates of the total film thickness obtained from the microscopic examinations, indi-

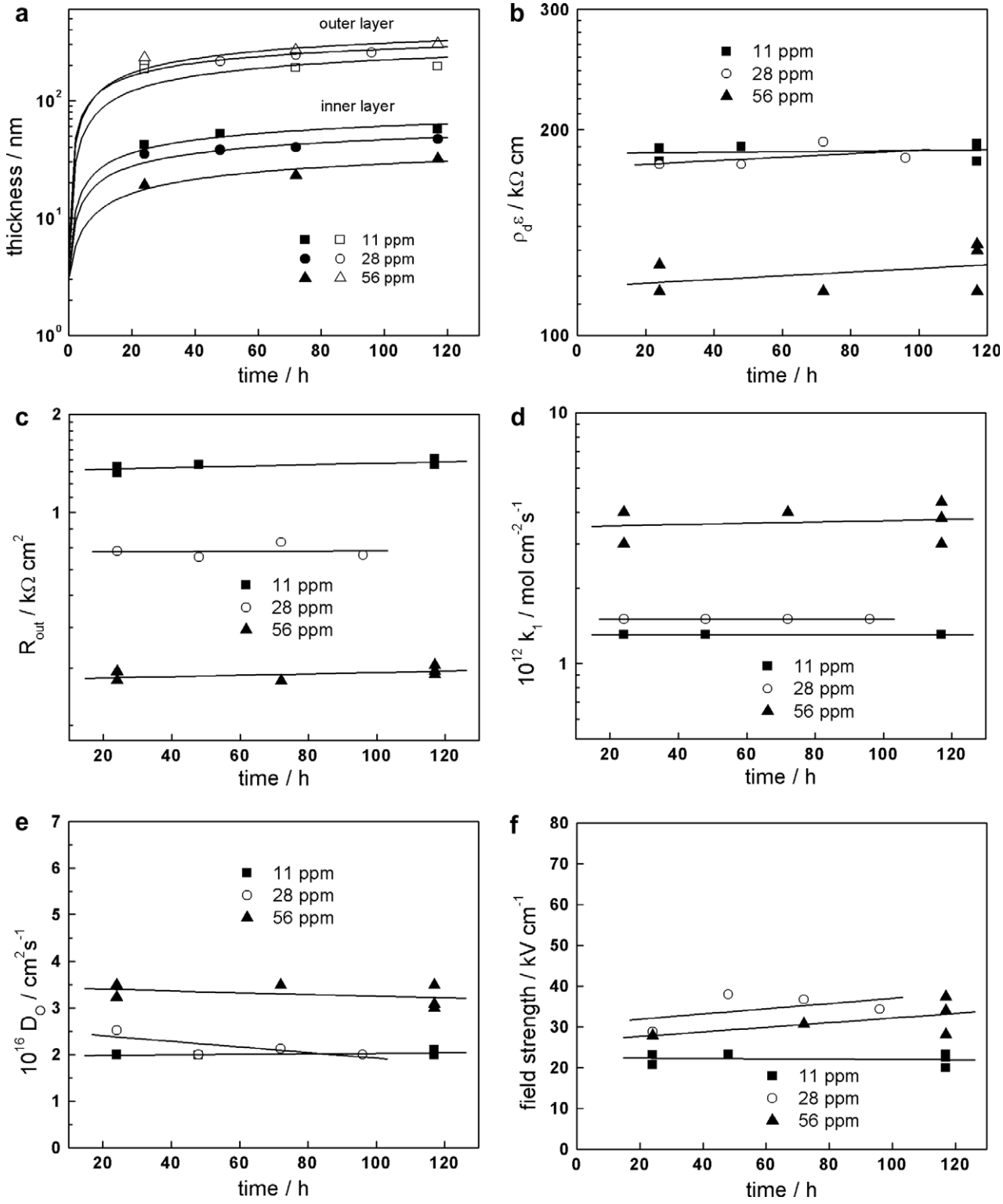

Fig. 8. Dependences of the (a) inner (full symbols) and outer (open symbols) layer thickness, (b) the parameter $\rho_d\varepsilon$, (c) the resistance of the outer layer R_{out}, (d) the rate constant of zirconium oxidation at the alloy/oxide interface k_1, (e) the diffusion coefficient of oxygen vacancies D_O and (f) the field strength in the inner layer $\vec{E}$ on the time of exposure of alloy E110 to the simulated WWER water with variable KOH content.

cating the validity of the proposed model for the oxide film. The thickness of the inner layer is several times smaller than that of the outer layer, which indicates that the corrosion properties of the zirconium alloys are controlled by a thin layer close to the alloy/oxide interface. The thicknesses of both layers seem to increase with time of exposure according to a direct logarithmic law (solid lines in Figs. 8(a)–9(a)). As such a law for film growth has been derived both from the PDM and the MCM [30], the evolution of oxide thickness with time can be taken as another proof for the adequacy of the representation of the corrosion processes using the MCM. The thickness of the whole oxide and the outer layer is larger on Zircaloy 4 when compared to E110 and in general increases with KOH concentration. On the other hand, the thickness of

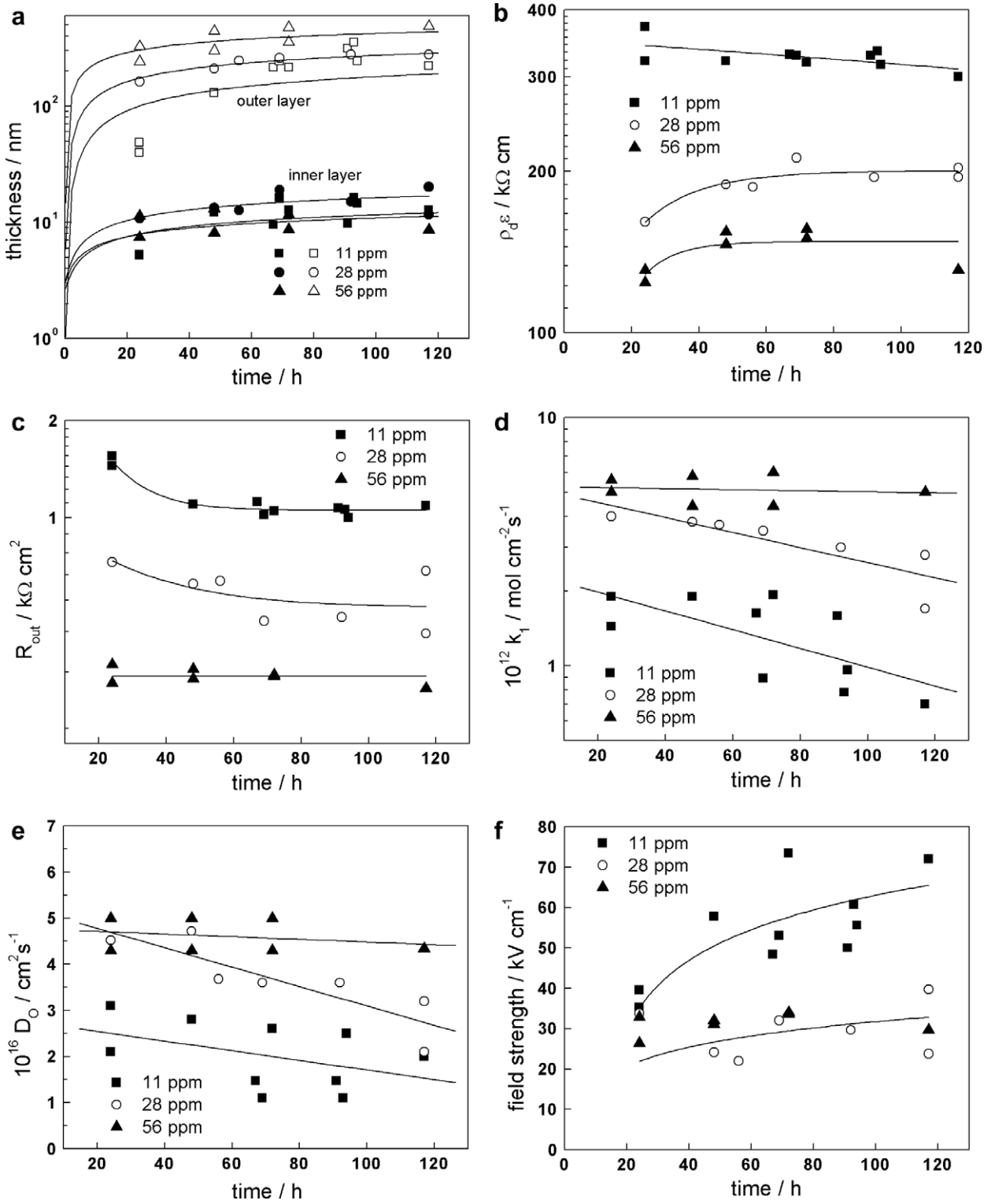

Fig. 9. Dependences of the (a) inner (full symbols) and outer (open symbols) layer thickness, (b) the parameter $\rho_d\varepsilon$, (c) the resistance of the outer layer R_{out}, (d) the rate constant of zirconium oxidation at the alloy/oxide interface k_1, (e) the diffusion coefficient of oxygen vacancies D_O and (f) the field strength in the inner layer $\vec{E}$ on the time of exposure of Zircaloy 4 to the simulated WWER water with variable KOH content.

the inner layer is somewhat smaller on Zircaloy 4 than on E110 and tends to decrease with increasing KOH concentration, which points out to the different properties of the inner layer on the two alloys.

- The values of the parameter $\rho_d\varepsilon$ that characterise the defect induced conductivity of the interface at which oxygen vacancies are generated (the alloy/oxide interface), preserve more or less constant values with exposure time and decrease with increasing KOH concentration (Figs. 8(b)–9(b)). Bearing in mind the expression for ρ_d given above, this behaviour may be correlated to the respective increase of the rate constant of generation of oxygen vacancies, k_1 (Figs. 8(d)–9(d)) with KOH concentration, assuming that the diffusion coefficient of electronic charge carriers does not change appreciably with KOH

concentration. The increase of k_1 with KOH concentration is most probably due to the increase of the rate of dissolution, k_d, with KOH concentration, as speculated already above. Indeed, in order to preserve the steady-state, if the rate of dissolution increases, so should the rate of transport through the oxide and the rate of oxidation at the alloy/barrier layer interface. The processes at the two interfaces and in the film bulk are related through the continuity in concentration of the major ionic current carriers, the oxygen vacancies. No meaningful differences between the values of $\rho_d\varepsilon$ are found for the two alloys, which is in line with the statement that conduction in the barrier layer at the interface with the alloy is governed by generation and transport of oxygen vacancies.

- For the oxide on Zircaloy 4 at a KOH concentration of 11 and 28 ppm, both the diffusion coefficient in the barrier layer and the rate constant of Zr oxidation decrease with oxidation time (Fig. 9(d)–(e)) Within the frames of the proposed approach. this observation can be tentatively explained by the deceleration of the dissolution rate of the oxide with time of exposure.
- The resistance of the outer layer R_{out}, (Figs. 8(c)–9(c)) does not depend on the type of alloy either but decreases significantly with increasing KOH concentration which may be related to an increased number of defects and short circuit conduction paths through this layer when the alloys are exposed to WWER water with higher KOH content. The respective resistivities calculated by dividing R_{out}, by the outer layer thickness decrease by a factor of 6–7 when the concentration of KOH in the electrolyte is increased 5 times, which may once more be connected to the quasi-linear increase of the solubility/dissolution rate with KOH concentration. Since the porosity of the outer layer has not been quantified in the present study, it is in principle possible that the decrease in the layer resistivity with increasing KOH concentration is due to the higher conductivity of the liquid in the pores of the outer layer.
- The diffusion coefficient of oxygen vacancies in the inner layer D_O (Figs. 8(e)–9(e)) does not change appreciably with exposure time and is reproducibly smaller for the oxide formed on E110 when compared to that on Zircaloy 4, which is in good accordance with the generally lower corrosion rate of E110, as observed experimentally. D_O in general increases with KOH concentration, i.e. the ionic conductivity of the inner layer seems also to be a function of KOH content in the WWER water. In line with the hypotheses proposed above, if oxide transformation via dissolution is rate limiting and depends on KOH concentration, in steady-state so should be the ionic conductivity and hence the diffusion coefficient. On the other hand, the field strength in the inner layer on Zircaloy 4 seems to decrease when the KOH content is increased from 11 to 28 ppm, whereas something of a reverse effect is observed for the inner layer on E110. In fact, the effect of KOH concentration on the field strength in the inner layer on E110 is on the overall small in comparison to that effect on the inner layer formed on Zircaloy 4. Clearly further studies are needed to explain this behaviour.

Summarising, it can be mentioned that the evolution of the estimated structural, kinetic and transport parameters with exposure time, KOH concentration and alloy type seems to be internally consistent and thus to furnish further proof for the validity of the proposed approach. As a next step in this investigation, the proposed model will be applied to data on the effect of Li content in simulated PWR water on the initial stages of oxidation of E110 in Zircaloy 4 in such medium. This study is relevant in order to understand why corrosion rates on Zr based alloys in KOH solutions (simulating VVER conditions) have been reported to be different from those measured in LiOH solutions of similar concentrations [31].

5. Conclusions

The experimental results obtained in the present work indicate that for both E110 and Zircaloy 4 in simulated WWER water, at the higher KOH concentration the oxidation is enhanced. Based on the interpretation of the impedance spectra through the mixed-conduction model the rate constant of Zr oxidation (generation of oxygen vacancies) at the alloy/film interface increases, the diffusion coefficient of oxygen vacancies in the barrier layer increases, both the defect induced resistivity of the inner layer and the overall resistivity of the outer layer decrease. Our hypotheses is that the effect of increasing KOH content in the electrolyte is to enhance the dissolution rate of the oxide, which in turn influences the rates of transport in the barrier layer and oxidation of Zr at the alloy/barrier layer interface. The process of dissolution at the oxide/electrolyte interface itself is not discernable in the impedance spectra probably because it is a chemical process that is not directly influenced by the potential drop through the oxide film. As an overall result, the changes in the above mentioned parameters lead to a film thickness increase with increasing KOH concentration. Based on these observations, it is predicted that in longer term exposures the oxide film thickness will have a higher growth rate in WWER water with a higher KOH content.

However, it is worth remembering that this study does not include all environmental effects (e.g. irradiation). Therefore the results presented in this paper can be considered only tentative with respect to actual in-reactor corrosion of zirconium alloys. Plans for the future studies on E110 and Zircaloy 4 include the comparison between the alkali hydroxides, i.e. LiOH vs. KOH, and also the effect of different anions, such as Cl^- or F^-. Concerning the modelling aspect of this work, it has been demonstrated that the MCM can be applied to reproduce quantitatively the initial stages of corrosion of zirconium alloys also in simulated WWER water. Thus, after taking into account irradiation effects, it can be used as a first approximation of a predictive model for the corrosion of such materials in nuclear power plants.

Acknowledgement

The funding of this work by SAFIR2010 – The Finnish Research Programme on Nuclear Power Plant Safety 2007–2010 is gratefully acknowledged.

References

[1] IAEA-TECDOC-996, Waterside Corrosion of Zirconium Alloys in Nuclear Power Plants, International Atomic Energy Agency, Vienna, 1998, p. 29.
[2] A.T. Fromhold Jr., Theory of Metal Oxidation – Vol. I. Fundamentals, North-Holland, Amsterdam, 1976.
[3] B.Cox, in Cox, in: M.G. Fontana, R.W. Staehle (Eds.), Advances in Corrosion and Corrosion Engineering, vol. 5, Plenum, NY, 1976, p. 173.
[4] B. Cox, J. Nucl. Mater. 336 (2006) 331.
[5] D.F. Taylor, J. Nucl. Mater. 184 (1991) 65.
[6] C. Bataillon, S. Brunet, Mater. Sci. Forum 111&112 (1992) 369.
[7] C. Bataillon, S. Brunet, Electrochim. Acta 39 (1994) 455.
[8] B. Cox, F. Gascoin, Y.-M. Wong, J. Nucl. Mater. 218 (1995) 113.
[9] B. Cox, Y.-M. Wong, J. Nucl. Mater. 218 (1995) 324.
[10] J. Schefold, D. Lincot, J.C. Badot, O. Kerrec, in: P. Natishan, H. Isaacs, M. Janik-Czachor, V. Macagno, P. Marcus, M. Seo (Eds.), Passivity andIts Breakdown, The Electrochemical Society Proceedings, vol. 97-26, 1998, p. 740.
[11] J.J. Vermoyal, A. Frichet, L. Dessemond, A. Hammou, Electrochim. Acta 45 (1999) 039.
[12] P. Barberis, A. Frichet, J. Nucl. Mater. 273 (1999) 182.
[13] J.J. Vermoyal, L. Dessemond, A. Hammou, A. Frichet, J. Nucl. Mater. 288 (2001) 297.
[14] M. Oskarsson, E. Ahlberg, U. Andersson, K. Petersson, J. Nucl. Mater. 297 (2001) 77.

[15] G. Nagy, Z. Kerner, T. Pajkossy, J. Nucl. Mater. 300 (2002) 230.
[16] G. Nagy, R. Schiller, Phys. Chem. Chem. Phys. 4 (2002) 791.
[17] J. Schefold, D. Lincot, A. Ambard, O. Kerrec, J. Electrochem. Soc. 150 (2003) B451.
[18] J.J. Vermoyal, A. Hammou, L. Dessemond, A. Frichet, Electrochim. Acta 47 (2002) 2679.
[19] R. Schiller, J. Balog, G. Nagy, J. Chem. Phys. 123 (2005) 094704.
[20] M. Bojinov, L. Hansson-Lyyra, P. Kinnunen, T. Saario, P. Sirkia, J. ASTM Int. 2 (2005) JAI12820.
[21] S. Forsberg, E. Ahlberg, M. Limbäck, J. ASTM Int. 4 (2007) JAI101123.
[22] J. Ai, Y. Chen, M. Urquidi-Macdonald, D.D. Macdonald, J. Electrochem. Soc. 154 (2007) C43.
[23] J. Ai, Y. Chen, M. Urquidi-Macdonald, D.D. Macdonald, J. Electrochem. Soc. 154 (2007) C52.
[24] B. Beverskog, M. Bojinov, P. Kinnunen, T. Laitinen, K. Makela, T. Saario, Corros. Sci. 44 (2002) 1923.
[25] M. Bojinov, P. Kinnunen, K. Lundgren, G. Wikmark, J. Electrochem. Soc. 152 (2005) B250.
[26] A.J. Markworth, A. Sehgal, G. Frankel, J. Electrochem. Soc. 146 (1999) 3672.
[27] O. Pensado, M. Urquidi-Macdonald, D.D. Macdonald, J. Electrochem. Soc. 148 (2001) B386.
[28] S. Havriliak, S. Negami, J. Polym. Sci. C 14 (1966) 99.
[29] J.R. Macdonald, J. Chem. Phys. 84 (1986) 496.
[30] M. Bojinov, A. Galtayries, P. Kinnunen, A. Machet, P. Marcus, Electrochim. Acta 52 (2007) 7475.
[31] Y.H. Jeong, J.H. Baek, S.J. Kim, H.G. Kim, H. Ruhmann, J. Nucl. Mater. 270 (1999) 322.